ISSN 8756-6990, Optoelectronics, Instrumentation and Data Processing, 2019, Vol. 55, No. 4, pp. 356–363. © Allerton Press, Inc., 2019.
Russian Text © The Author(s), 2019, published in Avtometriya, 2019, Vol. 55, No. 4, pp. 49–56.

AUTOMATION SYSTEMS IN SCIENTIFIC RESEARCH AND INDUSTRY

Simulation of Hybrid Unmanned Aerial Vehicle Motion

S. A. Belokon[a], D. S. Derishev[b], Yu. N. Zolotukhin[a*], and A. P. Yan[a]

[a] *Institute of Automation and Electrometry, Siberian Branch, Russian Academy of Sciences, pr. Akademika Koptyuga 1, Novosibirsk, 630090 Russia*
[b] *Novosibirsk Research Institute of Aviation Technology and Production Engineering, ul. Polzunova 15, Novosibirsk, 630051 Russia*
[*] *E-mail: zol@idisys.iae.nsk.su*

Received May 29, 2019; revision received June 11, 2019; accepted for publication June 11, 2019

Abstract—Performance of a hybrid unmanned aerial vehicle is analyzed. A mathematical model in MATLAB/Simulink is described. Results obtained by means of hardware-in-the-loop simulations and confirming the efficiency of the proposed control method are reported.

Keywords: hybrid unmanned aerial vehicle, hardware-in-the-loop, transitional modes.

DOI: 10.3103/S8756699019040058

INTRODUCTION

Results of analyzing the flight behavior of a hybrid unmanned aerial vehicle (UAV) with two types of engines (lifting and main engines) were reported in [1]. A mathematical model of the UAV was developed, and methods of UAV control at different stages of its flight were described, in particular, in the transitional mode from hovering to horizontal flight accompanied by a change in the lift force source: from quadrotor thrust to flight aerodynamics.

The present work is aimed at studying the behavior of the LL-100 hybrid UAV with the use of the general mathematical model and the laws of hybrid UAV control [1].

At the first stage of the hybrid UAV investigation, a mathematical model of the LL-100 UAV was developed, its behavior in the calm atmosphere was considered, and interaction of the propulsion subsystems during UAV flight was analyzed, especially in transitional modes: from vertical take-off to horizontal flight and from horizontal flight to vertical landing. The simulations were performed in MATLAB/Simulink at the hardware-in-the-loop platform based at the Institute of Automation and Electrometry of the Siberian Branch of the Russian Academy of Sciences [2].

UNMANNED AERIAL VEHICLE

A prototype of a hybrid UAV was developed for solving nontrivial scientific and engineering problems for unmanned aerial vehicles designed to be used outside the airdrome. The ultimate goal was the development of special and dual-use high-technology products. The general view of the UAV is shown in Fig. 1. The main mass, size, and flight parameters of the UAV are listed in Table 1.

SIMULATIONS

Simulation Platform

The present study was performed on the hardware-in-the-loop platform for investigating UAV control systems [2]. This platform provides various functions for developing a mathematical model of an object, studying the performance of the control system under various flight conditions, creating algorithms and software for the ground control station and airborne electronic equipment, and visualizing the 3D UAV model and cockpit external environment on flight simulators.

Fig. 1.

Table 1

UAV characteristics	Values
Take-off weight (kg)	30
Cruising velocity (m/s)	40
Stalling velocity (m/s)	20
Maximum velocity (m/s)	50
Position of the center of mass (at the OX axis)	30% MAC
Wing span (m)	3.1
Wing area (m^2)	1.112
Mean aerodynamic chord of the wing (MAC) (m)	0.37
Moments of inertia with respect to the axis ($kg \cdot m^2$):	
OX	5.5
OY	10.7
OZ	8.5

Specific features of the hardware-in-the-loop platform developed at the Institute of Automation and Electrometry of the Siberian Branch of the Russian Academy of Sciences are the built-in functions supporting the technology of dynamically scaled UAV models, in particular, supporting the analysis, comparisons, and iterative refinement of the mathematical description of the object based on flight test results, as well as performing hardware-in-the-loop simulations, which allows using both the onboard flight control and navigation equipment and the ground control station for real-time recording and displaying of telemetry data and verifying the system operation as a whole.

The structural scheme of the hardware-in-the-loop platform is presented in Fig. 2 (the communication lines involved into software and hardware testing are marked by the blue color, and the video channel from the camera to the aircraft nose model is marked by the green color). The following notations are used: ground control station (GCS), automated workstation (WKS), automatic control system (ACS), and flight control and navigation equipment (FCNE).

Propulsion Subsystems of the LL-100 UAV. Main Engine

The aircraft mode of UAV flight is ensured by the main engine consisting of a Double AXI 5345/16 HD Gold Line electrical motor rotating a two-blade pusher propeller 0.5 m in diameter with the slope of the blade cross section on the normalized radius $\bar{r} = 0.75$ ($\varphi_{0.75} = 21^\circ$). Figure 3 shows the aerodynamic characteristics (experimental data) of the propeller $\alpha = f(\lambda)$ and $\beta = f(\lambda)$ ($\lambda = V_x/(n_c D)$ is the normalized pitch of the propeller).

The thrust force of the main engine is directed along the propeller rotation axis and is equal [3–5] to $P_x^E = \alpha \rho n_E^2 D_E^4$, where P_x^E is the thrust force, α is the thrust coefficient, ρ is the air density, n_E is the number of turns of the propeller per minute, and D_E is the propeller diameter.

In calculating the moments generated by the main engine, it is taken into account that the propeller rotation axis coincides with the OX axis of the body-fixed system, whereas the gyroscopic moment generated

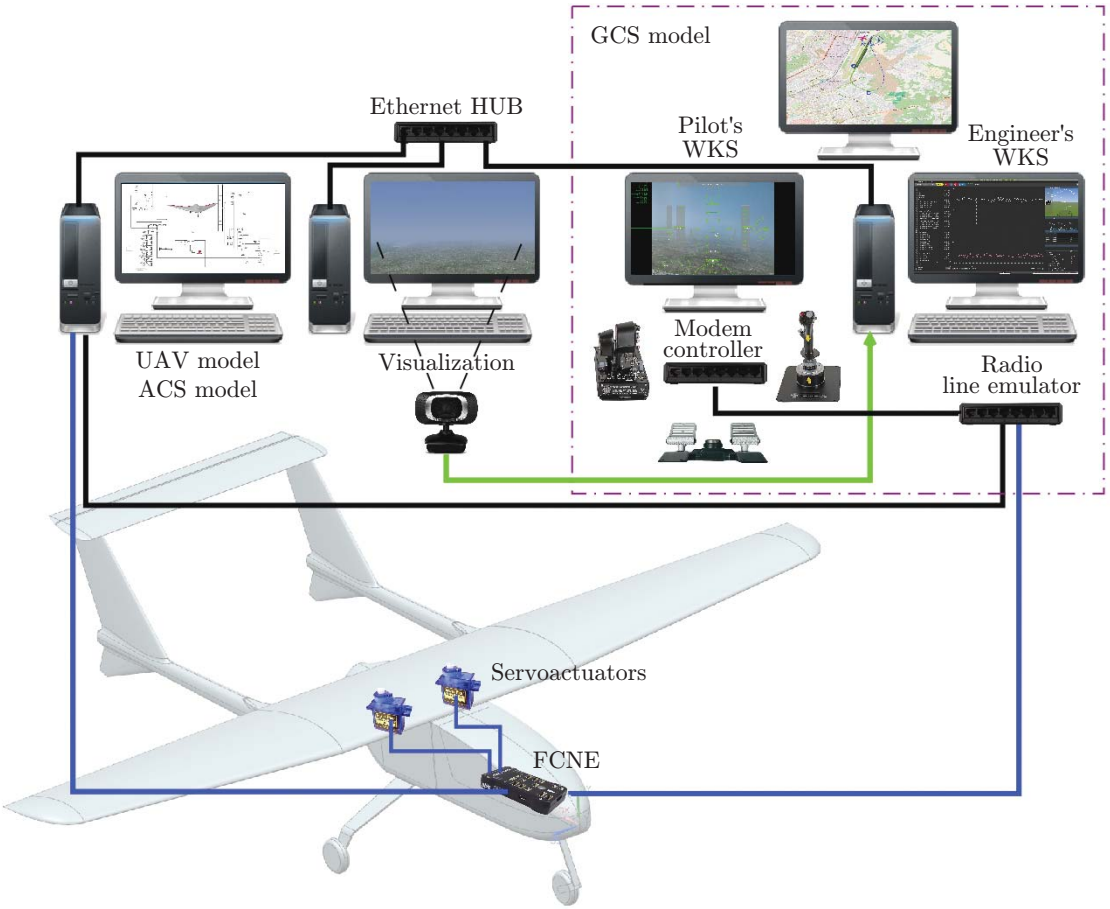
GCS model
Ethernet HUB
Pilot's
WKS
Engineer's
WKS
UAV model
ACS model
Visualization
Modem
controller
Radio
line emulator
Servoactuators
FCNE

Fig. 2.

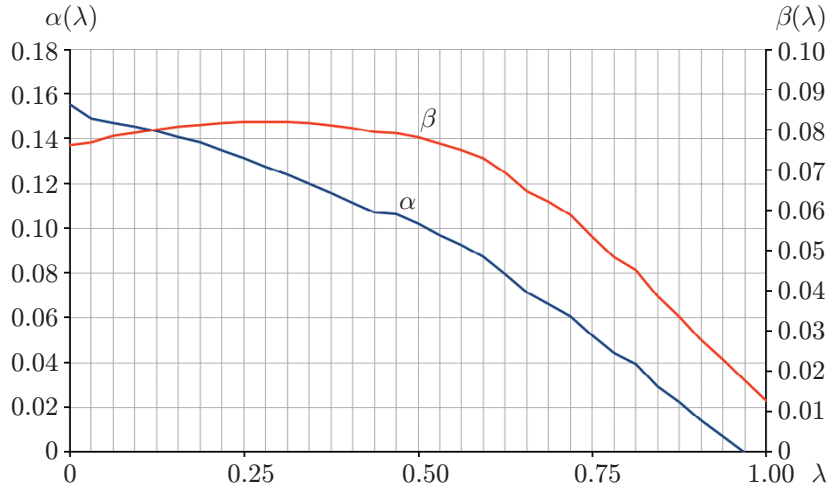
α(λ)
β(λ)
0.18
0.16
0.14
0.12
0.10
0.08
0.06
0.04
0.02
0
0.10
0.09
0.08
0.07
0.06
0.05
0.04
0.03
0.02
0.01
0
0
0.25
0.50
0.75
1.00
λ
β
α

Fig. 3.

Table 2

Rotation velocity, rpm	Power, W	Thrust, G
1000	0	0
2860	4590	505
3600	6700	915
3900	8100	1250
4300	9640	1675
4600	12235	2370

by the main engine is negligibly small. Thus, only the reactive moment is taken into account:

$$M_x^E = \frac{\beta\rho n_E^2 D_E^5}{2\pi}$$

(β is the power coefficient).

Lifting (Quadrotor) Propulsion Subsystem

To ensure vertical take-off and landing, the UAV considered in the present study is equipped with a lifting propulsion subsystem consisting of four rotors, each including a two-blade air propeller 0.65 m in diameter with the blade mounting angle $\varphi_{0.75} = 8^\circ$ and a TMotor U11 KV120 electrical motor. To compensate for the total reactive moment, propellers *1* and *2* rotate in the counterclockwise direction, whereas propellers *3* and *4* rotate in the clockwise direction (see Fig. 2 in [1]).

The throttling characteristics of one rotor (experimental data) are summarized in Table 2 in the form of the thrust and consumed power as functions of the number of turns.

The thrust generated by the propeller depends on the number of turns and UAV velocity [1, 3–5]:

$$P_y^Q = P_y^Q(0)\Big(1 + 0.1\,\frac{[[\mathbf{L}\otimes\boldsymbol{\omega}] - \mathbf{V}]_y}{n_Q D_Q}\Big).$$

Here P_y^Q is the thrust force generated by one rotor, $P_y^Q(0)$ is the thrust force of motionless propellers, $\mathbf{L}$ is the vector of distances from the rotation axes to the rotors, $\boldsymbol{\omega}$ and $\mathbf{V}$ are the angular and linear velocities of the UAV, respectively, n_Q is the number of propeller turns per minute, and D_Q is the diameter of the propeller of the lifting propulsion subsystem.

The total moment of forces acting on the UAV due to operation of propellers is the sum of the gyroscopic M_Q^{gyro} and reactive M_Q^r moments of the lifting propellers and also of the moment generated by the thrust force M_Q^P:

$$M_Q = \sum_{i=1}^{4} M_Q^{gyro}(i) + M_Q^r(i) + M_Q^P(i).$$

Here $M_Q^r(i) = [0\ N(i)/2(\pi n_Q(i))\ 0]$, $N = \beta\rho n_Q^3 D_Q^5$ is the power consumed by the propeller, $M_Q^{gyro}(i) = 2\pi n_Q(i) J(i)[\omega_z\ 0\ \omega_x]^\top$, J is the moment of inertia of the rotor, and $M_Q^P(i) = \beta\rho n_Q^2(i) D_Q^4/(2\pi)$.

For the arrangement of the quadrotor subsystem motors illustrated in Table 3, the forces and moments are defined as

$$\begin{bmatrix} P_y^Q \\ M_x^Q \\ M_y^Q \\ M_z^Q \end{bmatrix} = \begin{bmatrix} 1 & 1 & 1 & 1 \\ -z(1) & z(2) & z(3) & -z(4) \\ -\lambda & -\lambda & \lambda & \lambda \\ x(1) & -x(2) & x(3) & -x(4) \end{bmatrix} \begin{bmatrix} P_y^Q(1) \\ P_y^Q(2) \\ P_y^Q(3) \\ P_y^Q(4) \end{bmatrix},$$

where $z(i)$ and $x(i)$ are the distances from the axis of the propellers (i) to the rotation axes x and z, respectively, and λ is the coefficient of proportionality between the propeller thrust and reactive moment of rotation generated by the propeller.

Table 3

Number of the rotor	Coordinates, mm	
	$x(i)$	$z(i)$
1	545	510
2	−600	−510
3	545	−510
4	−600	510

Mathematical Model for the LL-100 UAV

A specific feature of the hybrid UAV under study is the possibility of using the thrust in the direction of the OX axis generated by the main engine of the UAV (P_x^E), and also the thrust in the direction of the OY axis generated by the quadrotor subsystem (P_y^Q):

$$\bar{F} = \bar{F}^E + \bar{F}^Q, \qquad \bar{F}^E = \begin{bmatrix} P_x^E \\ 0 \\ 0 \end{bmatrix}, \qquad \bar{F}^Q = \begin{bmatrix} 0 \\ P_y^Q \\ 0 \end{bmatrix}.$$

Then the system of equations of motion of the hybrid UAV (Eq. (3) from [1]) is modified in accordance with the specific features of the UAV under study:

$$m\Big(\frac{dV_x}{dt} + \omega_y V_z - \omega_z V_y\Big) = P_x^E - X - mg\sin\theta,$$

$$m\Big(\frac{dV_y}{dt} + \omega_z V_x - \omega_x V_z\Big) = P_y^Q + Y - mg\cos\theta\cdot\cos\gamma,$$

$$m\Big(\frac{dV_z}{dt} + \omega_x V_y - \omega_y V_x\Big) = Z + mg\cos\theta\cdot\sin\gamma,$$

$$I_x\frac{d\omega_x}{dt} - I_{xy}\Big(\frac{d\omega_y}{dt} - \omega_x\omega_z\Big) + (I_z - I_y)\omega_z\omega_y = M_x^Q + M_x^E,$$

$$I_y\frac{d\omega_y}{dt} - I_{xy}\Big(\frac{d\omega_x}{dt} + \omega_y\omega_z\Big) + (I_x - I_z)\omega_x\omega_z = M_y^Q,$$

$$I_z\frac{d\omega_z}{dt} + I_{xy}\Big(\omega_y^2 - \omega_x^2\Big) + (I_y - I_x)\omega_y\omega_x = M_z^Q,$$

$$\frac{d\gamma}{dt} = \omega_x - (\omega_y\cos\gamma - \omega_z\sin\gamma)\tan\theta,$$

$$\frac{d\theta}{dt} = \omega_z\cos\gamma + \omega_y\sin\gamma, \qquad \frac{d\psi}{dt} = \frac{1}{\cos\theta}(\omega_y\cos\gamma - \omega_z\sin\gamma),$$

$$\frac{dX_g}{dt} = V_x\cos\theta\cdot\cos\psi - V_y(\cos\gamma\cdot\sin\theta\cdot\cos\psi - \sin\gamma\cdot\sin\psi) + V_z(\cos\gamma\cdot\sin\psi + \sin\gamma\cdot\sin\theta\cdot\cos\psi),$$

$$\frac{dH}{dt} = V_x\sin\theta + V_y\cos\gamma\cdot\cos\theta - V_z\sin\gamma\cdot\cos\theta,$$

$$\frac{dZ_g}{dt} = -V_x\cos\theta\cdot\cos\psi + V_y(\cos\gamma\cdot\sin\theta\cdot\sin\psi - \sin\gamma\cdot\cos\psi) + V_z(\cos\gamma\cdot\cos\psi - \sin\gamma\cdot\sin\theta\cdot\sin\psi).$$

Here we use the standard notations [6] for the motion parameters, inertia and mass characteristics, forces, and moments of the UAV.

The equations used for estimating the aerodynamic forces and moments with allowance for the specific features of the LL-100 UAV are transformed to

$$F_x^A = ma_x - P_x^E, \qquad F_y^A = ma_y - P_y^Q, \qquad F_z^A = ma_z,$$

$$M_x^A = [I_x\dot{\omega}_x - I_{xy}(\dot{\omega}_y - \omega_x\omega_z) + (I_z - I_y)\omega_y\omega_z - (M_x^E + M_x^Q)],$$

$$M_y^A = [I_y\dot{\omega}_y + I_{xy}(\dot{\omega}_x + \omega_y\omega_z) + (I_x - I_z)\omega_x\omega_z - M_y^Q],$$

$$M_z^A = [I_z\dot{\omega}_z + I_{xy}(\omega_x^2 - \omega_y^2) + (I_x - I_y)\omega_x\omega_y - M_z^Q].$$

SIMULATION RESULTS

The control system was simulated in the MATLAB/Simulink environment with the following values of parameters: specified height above the underlying surface $h_{ref} = 15$ m, UAV mass $m = 30$ kg, initial roll angle $\gamma_{ref} = 0$, initial pitch angle $\theta_{ref} = 0$, and initial yaw angle $\psi_{ref} = 0$.

Experiment

As an example, we show the results of simulating the processes of vertical take-off, hovering, transition to horizontal flight, horizontal flight, transition to hovering, hovering above the landing site, vertical descent, and landing.

Figure 4 illustrates the behavior of some variables characterizing the UAV state: flight altitude (Altitude), lift force of the quadrotor subsystem (F_quad), aerodynamic lift force (F_aero), indicated air speed (IAS), angle of attack (α), and Euler angle (Euler). For convenience, the process is divided into several flight phases.

The first phase (vertical take-off) begins at the time $t = 0$ s when the lifting propulsion subsystem is actuated and is finalized when a specified height $h_{ref} = 15$ m is reached approximately at the time $t = 40$ s. At this instant of time, the second phase (hovering) begins, which is finalized at the time $t = 100$ s when the main engine is actuated. The third phase (transition to horizontal flight) is characterized by an increase in the flight velocity and, as a consequence, by an increase in the aerodynamic lift force, which has to replace the lift force generated by the quadrotor. By the time $t = 400$ s, the replacement is finalized, and the UAV passes to the fourth stage (horizontal flight). It should be noted that the transitional mode is not accompanied by the loss of the flight altitude, which is an undesirable phenomenon. At the time $t = 500$ s, the main engine is switched off, and the fifth stage begins (transition to hovering above the landing site), which is finalized approximately at $t = 800$ s. The sixth phase (hovering above the landing site) lasts until $t = 920$ s, when a command for landing is issued ($h_{ref} = 0$ m). During the seventh stage (vertical descent and landing), the lifting propulsion subsystem is switched off when the UAV descends to $h = 0.5$ m, and the process is finalized.

Figure 5 shows an enlarged plot of the lift force generated by the quadrotor subsystem F_quad (curve *1*) and the aerodynamic lift force F_aero (curve *2*). Obviously, the sum of these forces is constant at each instant of time (except for the initial and final instants) and is equal to the UAV weight.

CONCLUSIONS

Simulations of the flight of the LL-100 hybrid unmanned aerial vehicle confirmed the efficiency of the control system proposed in [1] for transitional modes. The developed control method based, in particular, on real-time estimation of the aerodynamic forces and moments provided required characteristics of transitional modes.

Further research will be aimed at estimating the influence of external factors on the behavior of the hybrid UAV on the basis of simulations and flight tests.

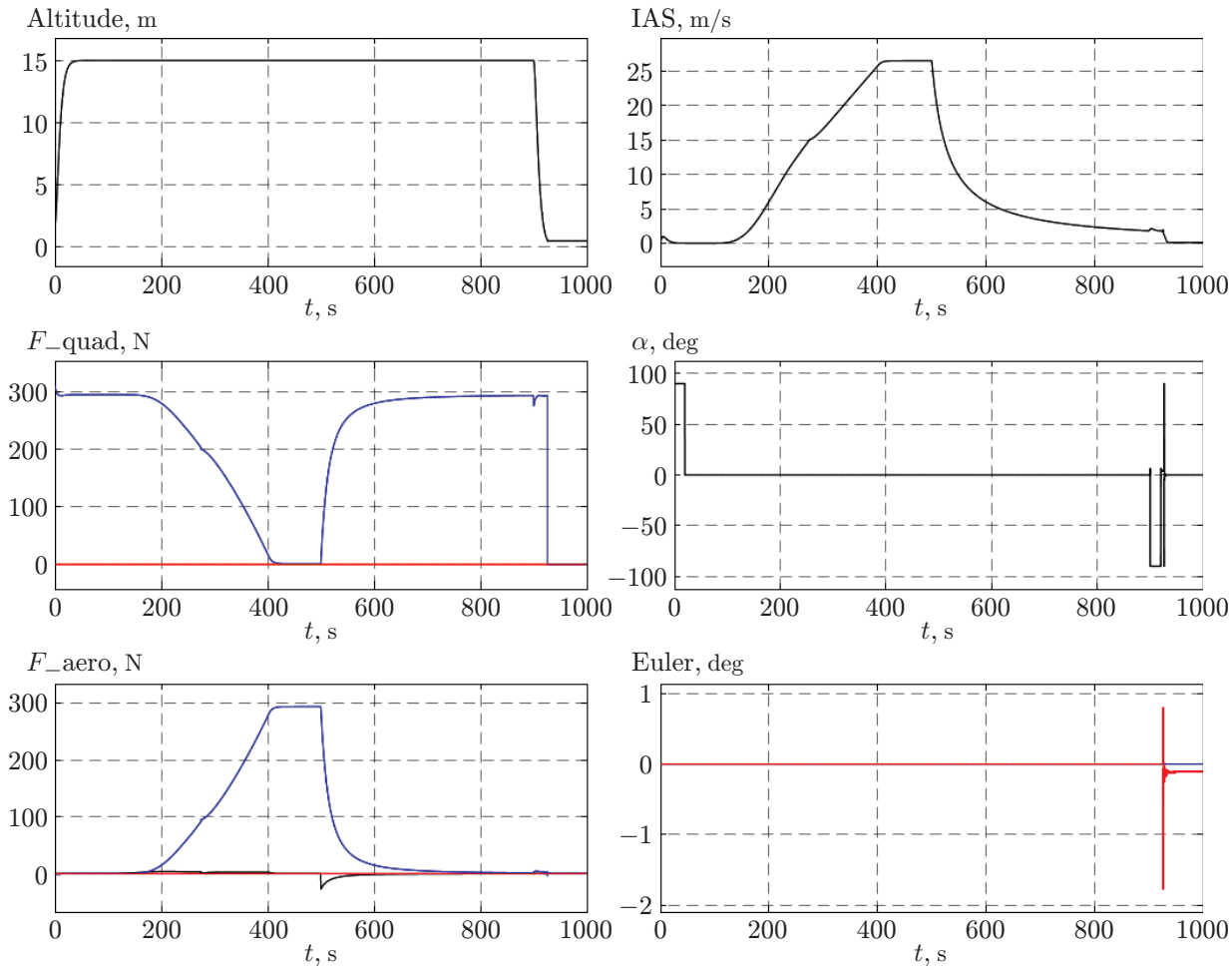

Fig. 4.

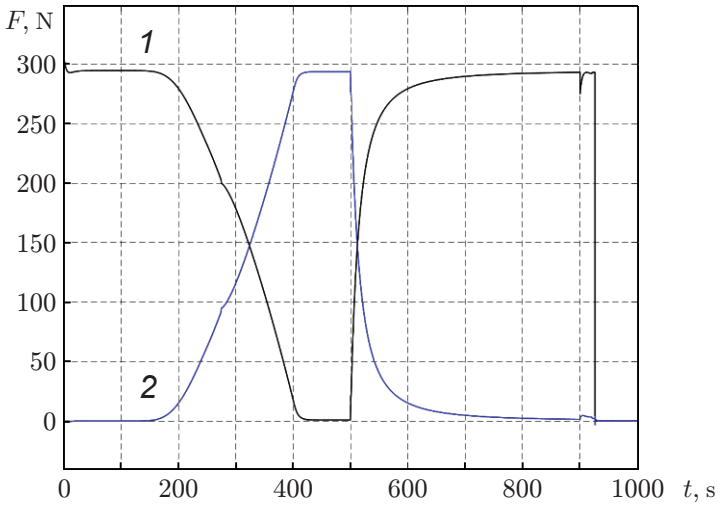

Fig. 5.

This work was partly supported by the Ministry of Science and Higher Education of the Russian Federation (State Registration No. AAAA-A17-117060610006-6).

REFERENCES

1. S. A. Belokon, D. S. Derishev, Yu. N. Zolotukhin, et al., "Control of Hybrid Unmanned Aerial Vehicle Motion in Transitional Modes," Avtometriya **55** (4), 37–48 (2019) [Optoelectron., Instrum., Data Process. **55** (4), 346–355 (2019)].
2. S. A. Belokon, Yu. N. Zolotukhin, and M. N. Filippov, "Architecture of a Platform for Hardware-in-the-Loop Simulation of Flying Vehicle Control System," Avtometriya **53** (4), 44–50 (2017) [Optoelectron., Instrum. Data Process. **53** (4), 345–350 (2017)].
3. A. S. Kravets, *Characteristics of Air Propellers* (Oborongiz, Moscow, 1941) [in Russian].
4. V. L. Teush and I. A. Sidorov, *General Course of Air Propellers* (Oborongiz, Moscow, 1943) [in Russian].
5. V. L. Aleksandrov, *Air Propellants* (Oborongiz, Moscow, 1951) [in Russian].
6. *Russian Standard GOST 20058-80, Dynamics of Aircraft in the Atmosphere* (Izd. Standartov, Moscow, 1981). http://gostexpert.ru/gost/getDoc/3780.